NASA Technical Memorandum 102683

CONICAL EULER SIMULATION AND ACTIVE SUPPRESSION OF DELTA WING ROCKING MOTION

ELIZABETH M. LEE
JOHN T. BATINA

OCTOBER 1990

National Aeronautics and Space Administration

Langley Research Center
Hampton, Virginia 23665

CONICAL EULER SIMULATION AND ACTIVE SUPPRESSION OF DELTA WING ROCKING MOTION

Elizabeth M. Lee and John T. Batina
NASA Langley Research Center
Hampton, Virginia 23665-5225

Summary

A conical Euler code was developed to study unsteady vortex-dominated flows about rolling highly-swept delta wings, undergoing either forced or free-to-roll motions including active roll suppression. The flow solver of the code involves a multistage Runge-Kutta time-stepping scheme which uses a finite-volume spatial discretization of the Euler equations on an unstructured grid of triangles. The code allows for the additional analysis of the free-to-roll case, by including the rigid-body equation of motion for its simultaneous time integration with the governing flow equations. Results are presented for a 75° swept sharp-leading-edge delta wing at a freestream Mach number of 1.2 and at α = 10° and 30° angle of attack. At the lower angle of attack of α = 10°, a forced harmonic analysis indicates that the rolling moment coefficient provides a positive damping which is verified in a free-to-roll calculation. In contrast, at the higher angle of attack of α = 30°, a forced harmonic analysis indicates that the rolling moment coefficient provides a negative damping at the small roll amplitudes. A free-to-roll calculation for this case produces an initially divergent response, but as the amplitude of motion grows with time, the response transitions to a wing-rock type of limit cycle oscillation. The wing rocking motion may be actively suppressed, however, through the use of a rate-feedback control law and antisymmetrically-deflected leading-edge flaps. The paper provides descriptions of the conical Euler flow solver and the free-to-roll analysis. Results are presented which give insight into the flow physics associated with unsteady vortical flows about forced and free-to-roll delta wings, including the active roll suppression of this wing-rock phenomenon.

Introduction

In recent years, the understanding and prediction of the complex flows about modern aircraft at high angles of attack have been research topics that have generated much interest within the fluid dynamics community.[1,2] These aircraft typically have thin highly-swept lifting surfaces which produce a vortical flow over the leeward-side of the vehicle at high angles of attack. This vortical flow can have beneficial effects on performance, such as lift augmentation at high-α, but may also have adverse effects such as structural fatigue due to tail buffet and also stability and control problems such as wing rock, wing drop, nose slice, and pitch-up.[3] Consequently, considerable work has been done experimentally to try to understand the basic flow physics involved in vortical flows about delta wings at high angles of attack. Experimental research efforts directed towards understanding and documenting steady vortical flows are typified by the detailed flowfield measurements about simple, cranked, and canard-wing delta configurations at low speed by Hummel[4] and low speed tests on a 75° swept delta wing by Kjelgaard and Sellers.[5] For supersonic-freestream Mach numbers, vortical flows have been measured by Squire[6] for an elliptic cone delta wing and by Miller and Wood[7] for a series of swept sharp-leading-edge delta wings. Efforts on investigating unsteady vortical flows experimentally have been reported by Nguyen et al.[8] for forced harmonic and free-to-roll motions of an 80° swept delta wing in low speed flow. In Ref. 8, the wing was found to undergo self-induced periodic roll oscillations known as wing rock, for angles of attack greater than 25°. Levin and Katz[9] tested both 76° and 80° swept delta wings and found that only the 80° model would exhibit wing rock at high-α. Further studies have been performed by Nelson and co-workers[10,11] at Notre Dame University. These studies have shown, for example, the time histories of the vortex core position during a cycle of wing rock[10] and the static and dynamic effects due to vortex breakdown.[11] Also Ng et al.[12] have recently reported experimental results obtained in a water tunnel which show wing rock for several different delta wing planforms along with detailed flow visualization diagrams. These studies[4-12] have contributed

significantly to the understanding of steady and unsteady vortex-dominated flowfields, although much work remains to be done.

From a computational point of view, considerable effort has also been spent on developing methods of predicting steady and unsteady vortex-dominated flows.[13,14] Hoeijmakers,[13] for example, gives a review of computational methods for the determination of steady vortical flow characteristics with an emphasis on classical methods including discrete vortex, cloud-in-cell, panel, vortex layer with finite core, leading-edge suction analogy, and vortex-lattice. With respect to unsteady methods, Hsu and Lan[15] presented a nonlinear mathematical model for calculating wing-rock characteristics based on aerodynamic derivatives evaluated using steady-flow aerodynamics at average dynamic conditions. Researchers at Virginia Polytechnic Institute and State University[16-18] have simulated wing rock using an unsteady vortex-lattice method to predict the aerodynamic loads and have integrated the equation of rolling motion using a predictor-corrector method. The methods of both Ref. 15 and Refs. 16-18 predicted with reasonable accuracy the low-speed wing rock characteristics of the delta wings studied in Refs. 8 and 9. Use of the more modern computational fluid dynamics (CFD) techniques for the prediction of vortex-dominated flows[14] have primarily focused on steady applications,[19-26] although there are notable exceptions where applications have been made to rolling delta wings undergoing forced harmonic[27-29] and free-to-roll[30] motions. Kandil and Chuang, for example, have reported results for rolling delta wings obtained using the conical Euler equations for sharp-leading-edge wings[27] and the conical Navier-Stokes equations for rounded-leading-edge wings.[28] Batina[29] has also presented results for a rolling delta wing obtained using a conical Euler flow solver based on the use of unstructured grids of triangles. Lee and Batina[30] extended the methods of Ref. 29 to include a free-to-roll capability and showed results for a freely rolling delta wing that exhibited a limit cycle or wing-rock type motion.

The objective of the current research is to study unsteady vortex-dominated flowfields by using the conical Euler equations as an efficient first step to investigating the full three-dimensional problem. Reference 30 reported the development of a conical Euler code to study unsteady vortex-dominated flows about rolling highly-swept delta wings undergoing forced harmonic and free-to-roll motions. The purpose of this paper is to report the extension of these methods for the study of flows about delta wings undergoing pulsed motions and free-to-roll motions including roll suppression. The flow solver of the code is similar to that of Ref. 29, which involves a multistage Runge-Kutta time-stepping scheme and a finite-volume spatial discretization of the Euler equations on an unstructured grid of triangles. The code was modified to allow for the additional analysis of the free-to-roll case, by including the rigid body equation of motion for its simultaneous time integration with the governing flow equations. The analysis also includes a capability for implementing an active feedback control law with antisymmetrically-deflected leading-edge flaps for roll suppression of the wing-rocking motion. Although limited experimental work has been conducted on the use of flaps[31] and leading edge blowing[32,33] for roll control, even less analytical and numerical work[34] has been performed. Results are presented here for a 75° swept sharp-leading-edge delta wing at a freestream Mach number of 1.2 and at α = 10° and 30° angle of attack. The results demonstrate the successful CFD simulation of a wing-rock phenomenon including its active roll suppression. The paper gives descriptions of the conical Euler flow solver and free-to-roll analysis. The results give insight into the flow physics associated with unsteady vortical flows about forced and free-to-roll delta wings, including the active roll suppression of this wing-rock phenomenon.

Symbols

a_∞ freestream speed of sound

C_ℓ rolling moment coefficient

C_{ℓ_δ} rolling moment coefficient transfer function due to flap deflection

C_{ℓ_ϕ} rolling moment coefficient transfer function due to roll

c root chord of wing

e total energy

i imaginary unit, satisfying the equation $i^2 = -1$

I_{xx} mass moment of inertia about longitudinal axis

k reduced frequency based on one half of the root chord, $\frac{\omega c}{2U_\infty}$

K_v control gain

ℓ rolling moment, positive clockwise when viewed from aft

M_∞ freestream Mach number

q_∞ freestream dynamic pressure

S planform area

$\bar{t}$ nondimensional time, $\frac{ta_\infty}{c}$

u component of velocity vector in x-direction

v component of velocity vector in y-direction

w component of velocity vector in z-direction

α angle of attack

γ ratio of specific heats

δ leading-edge flap deflection angle, positive clockwise when viewed from aft

$\Delta\bar{t}$ nondimensional time step

μ_x structural damping

ρ density

ρ_∞ freestream density

ϕ instantaneous roll angle, positive clockwise when viewed from aft

ϕ_o harmonic and pulse roll angle amplitude

Governing Equations

The flow is governed by the time-dependent Euler equations which may be written in conservation law form as

$$\frac{\partial Q}{\partial t} + \frac{\partial E}{\partial x} + \frac{\partial F}{\partial y} + \frac{\partial G}{\partial z} = 0 \qquad (1)$$

where Q is the vector of conserved variables defined by

$$Q = [\rho, \rho u, \rho v, \rho w, e]^T \qquad (2)$$

and E, F, and G are the convective or inviscid fluxes given by

$$E = \begin{bmatrix} \rho U \\ \rho U u + p \\ \rho U v \\ \rho U w \\ (e+p)U + x_t p \end{bmatrix} \qquad (3a)$$

$$F = \begin{bmatrix} \rho V \\ \rho V u \\ \rho V v + p \\ \rho V w \\ (e+p)V + y_t p \end{bmatrix} \qquad (3b)$$

$$G = \begin{bmatrix} \rho W \\ \rho W u \\ \rho W v \\ \rho W w + p \\ (e+p)W + z_t p \end{bmatrix} \qquad (3c)$$

The contravariant velocities U, V, and W are defined by

$$U = u - x_t \qquad V = v - y_t \qquad W = w - z_t \qquad (4)$$

where x_t, y_t, and z_t are the grid speeds in the x, y, and z directions, respectively. The pressure p is determined by the equation of state for a perfect gas

$$p = (\gamma - 1)\left[e - \frac{1}{2}\rho\,(u^2 + v^2 + w^2)\right] \tag{5}$$

and the equations have been nondimensionalized by the freestream density and the freestream speed of sound.

If interest is restricted to supersonic flow past conical bodies, then the conical flow assumption can be made. This reduces the problem from three dimensions to two dimensions, which significantly decreases the computational resources that are required to investigate such flows. The conical flow assumption is exact for steady inviscid supersonic flow. For unsteady flows, however, the conical assumption implies an instantaneous propagation of disturbances in radial directions. The conical flow assumption involves a change of variables according to

$$\xi = x \qquad \eta = \frac{y}{x} \qquad \zeta = \frac{z}{x} \tag{6}$$

The three-dimensional Euler equations then reduce to

$$\frac{\partial Q}{\partial t} + \frac{\partial}{\partial \eta}(F - \eta E) + \frac{\partial}{\partial \zeta}(G - \zeta E) + 2E = 0 \tag{7}$$

Equation (7) may be rewritten in integral form for solution as

$$\frac{\partial}{\partial t}\int_{\Omega} Q\, d\eta\, d\zeta + \int_{\partial\Omega}\left[(F - \eta E)\, d\zeta - (G - \zeta E)\, d\eta\right] + \int_{\Omega} 2E\, d\eta\, d\zeta = 0 \tag{8}$$

where the second integral is a boundary integral resulting from application of the divergence theorem.

Euler Solution Algorithm

The unsteady conical Euler equations are solved using the multistage Runge-Kutta time-stepping scheme of Ref. 29. This algorithm uses a finite-volume spatial discretization for solution on an unstructured grid made up of triangles. The original algorithm of Ref. 29 was a node-based scheme whereby the flow variables are stored at the vertices of the triangles. A second algorithm, a cell-centered scheme, was employed in the present study. This second scheme is based on unpublished work of the second author. In the cell-centered scheme, the flow variables are stored at the centroids of the triangles. In both algorithms, artificial dissipation is added explicitly to prevent oscillations near shock waves and to damp high-frequency uncoupled error modes. Specifically, an adaptive blend of harmonic and biharmonic operators is used, corresponding to second and fourth difference dissipation, respectively. The biharmonic operator provides a background dissipation to damp high frequency errors and the harmonic operator prevents oscillations near shock waves. The algorithms also employ enthalpy damping, local time stepping, and implicit residual smoothing to accelerate convergence to steady state. The local time stepping uses the maximum allowable step size at each grid point for the node-based scheme and for each triangle in the cell-centered scheme, as determined by a local stability analysis. The implicit residual smoothing permits the use of local time steps that are larger than those imposed by the Courant-Friedrichs-Lewy stability condition. This is achieved by averaging the residuals implicitly with neighboring values. A time-accurate version of the residual smoothing is also used for global time-stepping during unsteady applications of the code.

With respect to boundary conditions, freestream conditions are applied along the farfield boundary, and a reasonably large computational grid is used so that the bow shock is captured as a part of the solution. A flow tangency (or slip) condition is applied to the inner boundary which represents the wing. Also, for unsteady applications, the grid is moved to conform to the instantaneous position of the wing using a combination of rigid body rotation and deforming mesh movement. A deforming mesh algorithm

discussed below is used to deform the grid about the deflected leading-edge flaps in a wing-fixed coordinate system. This deformed mesh is then rotated as a rigid body to account for the instantaneous roll angle of the wing. In this application, grid speeds are computed at the nodes and are included in the governing equations to account for the relative motion between the grid and the fluid.

Deforming Mesh Algorithm

The deforming mesh algorithm as developed in Ref. 35, models the triangulated mesh as a spring network where each edge of a triangle represents a spring with stiffness inversely proportional to the square of its length. In this method, the grid points along the outer boundary are held fixed while the grid points along the wing (inner boundary) are specified. The locations of the interior points are then determined by solving the static equilibrium equations which result from a summation of forces at each node in both the η and ζ directions. The solution of the equilibrium equations is carried out using a predictor-corrector method which first predicts the new locations of the interior points by extrapolation from the previous time levels and then corrects these locations by using several Jacobi iterations of the static equilibrium equations. The predictor-corrector procedure is relatively efficient since it requires only a few Jacobi iterations to efficiently move the mesh.

Pulse Transfer-Function Analysis

Generally, unsteady load coefficients can be obtained by calculating several cycles of a harmonically forced oscillation with the determination of the load based on the last cycle of oscillation. This method of harmonic oscillation requires one flowfield calculation for each value of reduced frequency of interest. By contrast, the unsteady load coefficients may be determined for a wide range of reduced frequency in a single flowfield calculation using the pulse transfer-function analysis. The pulse transfer-function analysis has been employed in the past to determine the generalized

aerodynamic-forces (GAFs) which are used in aeroelastic analyses.[36,37] In the pulse analysis, the unsteady force coefficient is computed indirectly from the response of the flowfield due to a smoothly varying, exponentially-shaped pulse. Results computed using the pulse analysis for a pitching flat-plate airfoil were presented in Ref. 36. These results were in good agreement with parallel linear theory calculations which validated the accuracy of the analysis. Applications to transonic airfoil cases were also in good agreement with the GAFs computed using the harmonic method which tends to verify that the analysis is valid for predicting the small perturbation response about a nonlinear flowfield.[37] Therefore, because of the computational efficiency of the pulse transfer-function analysis, the capability was implemented within the conical Euler code to calculate the rolling moment coefficient due to roll, C_{ℓ_ϕ}, of a delta wing. The pulse is expressed as

$$\phi(\bar{t}) = \phi_0 e^{-M_\infty^2(\bar{t}-\bar{t}_c)^2} \qquad (9)$$

where ϕ_0 is the pulse amplitude, M_∞ is the freestream Mach number which determines the width of the pulse, and $\bar{t}_c$ is the nondimensional time at the center of the pulse. A small rolling pulse is prescribed for the delta wing, and the aerodynamic transient is calculated. The aerodynamic transient is then used to obtain the rolling moment coefficient in the frequency domain by a transfer-function analysis. In this case, a fast Fourier transform (FFT) of the rolling moment coefficient is divided by a FFT of the pulsed rolling motion. The transform assumes that the system is locally linear which is shown to be a valid assumption for the pulse amplitude of 1° used in the present study.

Free-to-Roll Analysis

In this section, the roll equation of motion, the time-marching solution procedure and the active roll suppression are described.

Roll Equation of Motion

The equation of motion for a rolling delta wing can be expressed as

$$I_{xx}\ \ddot{\phi} = \ell - \mu_x\ \dot{\phi} \tag{10}$$

where ϕ is the roll angle which is positive clockwise when viewed from aft, I_{xx} is the mass moment of inertia about the longitudinal axis, ℓ is the aerodynamic rolling moment also positive clockwise, and μ_x is a structural damping term (dot superscripts indicate differentiation with respect to time). In order to nondimensionalize Eq. (10), the angular rates are multiplied by the root chord of the delta wing, c, and divided by the freestream speed of sound, a_∞. The rolling moment coefficient is defined as

$$C_\ell = \frac{\ell}{q_\infty\, S\, c} \tag{11}$$

where q_∞ is the freestream dynamic pressure and S is the planform area. The nondimensional rolling equation of motion can then be written as

$$\phi'' = C_1\, C_\ell - C_2\, \phi' \tag{12}$$

where

$$C_1 = \frac{M_\infty^2\, S\, c^3\, \rho_\infty}{2\, I_{xx}} \tag{13a}$$

$$C_2 = \frac{\mu_x\, c}{a_\infty\, I_{xx}} \tag{13b}$$

Note that the prime superscripts indicate differentiation with respect to nondimensional time, $\bar{t}$. The structural damping term is added to simulate a sting bearing mount. This type of bearing mount was used in the low-speed wind tunnel investigations of wing rock reported in Refs. 8-11.

Time-Marching Solution

The solution procedure for the time integration of Eq. (12) is based on a finite difference representation of the time derivatives. The time derivatives are expressed in

terms of second-order-accurate finite-difference approximations. After substituting these expressions into Eq. (12), the roll angle at time level n+1 can be expressed in terms of the roll angle at previous time levels as

$$\phi^{n+1} = [C_1 C_\ell^{n+1} \Delta\bar{t}^2 + (5 + 2 C_2 \Delta\bar{t})\phi^n - (4 + \tfrac{1}{2} C_2 \Delta\bar{t})\phi^{n-1} + \phi^{n-2}] / [\tfrac{3}{2} C_2 \Delta\bar{t} + 2] \qquad (14)$$

The rolling moment at time level n+1, C_ℓ^{n+1}, is estimated from a linear extrapolation of C_ℓ at the previous two time levels. This predicted value of C_ℓ is used to determine the roll angle at time level n+1, ϕ^{n+1}. The flowfield is then calculated about the wing at this roll angle, and the actual value of the rolling moment coefficient is determined. The rolling moment coefficient is then updated for use in the next time step. Due to the explicit time-marching of the Euler code used in this study, the time steps required for stability were small, and thus, it was not necessary to iterate between the roll angle calculation and the flowfield calculation at each time step. Previous studies of time-marching aeroelastic analyses using a similar explicit scheme have shown this to be the case (R. D. Rausch: Personal Communication, October 31, 1989). For a free-to-roll calculation, steady-state initial conditions are specified for ϕ^{-1}, ϕ^0, C_ℓ^{-1}, and C_ℓ^0. An initial angular velocity is imposed to provide an initial perturbation to the wing.

Active Roll Suppression

Active roll suppression is achieved through the addition of an active rate-feedback control law to the time-marching solution procedure. A simple control law was chosen of the form

$$\delta = K_v \phi' \qquad (15)$$

where K_v is the control gain and δ is both the left and right leading-edge flap deflection angles measured positive clockwise from the flap hinge lines. The control law is applied to both left and right flaps simultaneously which results in an antisymmetric configuration. The time-marching solution procedure is the same as that which was

described in the preceding section. However, after the roll angle at time level n+1 is determined from Eq. (14), the flap deflection angle is determined from Eq. (15) using a second-order-accurate finite-difference expression for the angular velocity ϕ'. The deforming mesh algorithm is then applied in addition to the rigid rotation to move the mesh to its new position. As before, the flowfield is calculated about the wing at its new position, and the rolling moment coefficient is determined and then updated for use in the next time step. The same initial conditions as described in the preceding section are applied to begin the calculation.

Results and Discussion

Calculations were performed for a 75° delta wing at a freestream Mach number of 1.2 and at α = 10° and 30° angle of attack. The wing has thickness and sharp leading edges as indicated in the partial view of the grid shown in Fig.1. The thickness-to-span ratio at this cross section is 0.025 and the lower edge bevel angle is 10°. The grid, which was generated using an advancing front method,[38] has a total of 4226 nodes and 8299 elements. The grid was designed to be fine on the leeward side of the wing where the dominant flow features are expected to occur and to be coarse on the windward side of the wing where the flow gradients are expected to be small. As discussed previously, for unsteady applications, the mesh is rotated as a rigid body to conform to the instantaneous position of the main part of the wing. The mesh is deformed locally near the leading edges to conform to the instantaneous position of the flaps. As examples of mesh movement, partial views of the left leading-edge flap at a positive (δ = 10°) and a negative (δ = -10°) flap deflection angle are shown in Figs. 2(a) and 2(b), respectively, with the wing rotated through 10° of motion. The hinge point of the flap coincides with the inboard bevel edge and so the flap length is approximately 28% of the semi-span. As shown in the figure, the mesh moves smoothly as the wing rolls and the flaps are deflected.

Steady and unsteady results including the pulse, forced harmonic and free-to-roll calculations are presented for both α = 10° and 30°. The rate-feedback control law is applied to the α = 30° case since it was the only free-to-roll case to exhibit a wing-rock behavior.

Steady-State Results

Steady-state results were obtained to determine the basic character of the vortical flows and to provide starting solutions for the unsteady cases. A comparison of total pressure loss contours from these solutions, shown in Fig. 3, illustrates the effects of angle of attack. For the α = 10° angle of attack shown in Fig. 3(a), the contours indicate that the flow separates from each of the leading edges of the wing producing two small, widely-spaced circular vortices. In contrast, at the α = 30° angle of attack, shown in Fig. 3(b), the contours indicate that the flow separating from the leading edges produces two large, more closely-spaced circular vortices. Also, as the flow accelerates beneath the vortices of Fig. 3(b), vertically-oriented crossflow shock waves are formed on the outboard portions of the wing. Weaker shock waves are formed on the top of each vortex. These vertically-oriented shocks are located above the core of the vortex. A weaker horizontal shock wave is also present between the vortices.

Pulse Transfer-Function Results

The pulse transfer-function analysis was performed to determine the small amplitude stability and response characteristics of the wing. A stability analysis was derived by first recalling the nondimensional rolling equation of motion given by

$$\phi'' = C_1 C_\ell - C_2 \phi' \qquad (12)$$

For simplicity, the structural damping term (C_2) is set equal to zero resulting in

$$\phi'' = C_1 C_\ell \qquad (16)$$

Assuming that the rolling moment coefficient can be written as the product of the rolling moment coefficient transfer function C_{ℓ_ϕ} and the roll angle ϕ,

$$C_\ell = C_{\ell_\phi}\phi \tag{17}$$

then for simple harmonic motion

$$C_\ell = [\mathrm{Re}(C_{\ell_\phi}) + i\,\mathrm{Im}(C_{\ell_\phi})]\phi \tag{18}$$

where $\mathrm{Re}(C_{\ell_\phi})$ and $\mathrm{Im}(C_{\ell_\phi})$ represent the real and imaginary parts of the first harmonic component of C_{ℓ_ϕ}, respectively. In this case, the real part of the rolling moment coefficient transfer-function represents an aerodynamic stiffness and the imaginary part represents an aerodynamic damping. Therefore, for this simple one degree-of-freedom case, the sign of $\mathrm{Im}(C_{\ell_\phi})$ determines the stability in roll of the wing for small perturbations. In other words, a negative $\mathrm{Im}(C_{\ell_\phi})$ indicates a positive aerodynamic damping which would cause a free-to-roll wing to be stable, and a positive $\mathrm{Im}(C_{\ell_\phi})$ indicates a negative aerodynamic damping which would cause a free-to-roll wing to be unstable.

The pulse transfer-function analysis can be used to determine the rolling moment coefficient transfer-function and therefore the stability of the wing for a wide range of reduced frequency k (based on one-half of the wing root chord). A comparison of the pulse transfer-function analysis results, shown in Fig. 4, indicates the effects of angle of attack. At the lower angle of attack of α = 10° shown in Fig. 4(a), the $\mathrm{Im}(C_{\ell_\phi})$ is negative for all values of reduced frequency which is indicative of stability in roll for small perturbations. In contrast, at the higher α = 30° angle of attack shown in Fig. 4(b), the imaginary part is positive for $k \leq 0.5$ which is indicative of instability in roll. Also, for α = 30°, the $\mathrm{Re}(C_{\ell_\phi})$ is negative in this range of reduced frequency

which corresponds to a positive aerodynamic stiffness. The roll response will therefore oscillate (with increasing amplitude) rather than give rise to a static instability known as wing drop.

The accuracy of the pulse analysis is verified by harmonic analyses performed at five values of reduced frequency: k = 0.0, 0.25, 0.50, 0.75 and 1.0. In these analyses, the wing was oscillated harmonically in roll with an amplitude of 1° for three cycles of motion with the rolling moment coefficient determined from the last cycle. The results of the harmonic analyses are compared with the rolling moment coefficient transfer-functions in Fig. 4. The good agreement between pulse and harmonic analyses therefore validates the accuracy of the pulse results for the cases considered.

Forced Harmonic Results

Because the pulse transfer-function analysis is limited to small perturbations, the large perturbation aerodynamic characteristics of the delta wing were investigated with a forced harmonic analysis. A reduced frequency of k = 0.25 was chosen for this analysis. This value lies at the midpoint of the range of reduced frequency identified by the pulse analysis as being an unstable condition for the free-to-roll wing at α= 30°. Three amplitudes of motion, ϕ_0 = 5°, 15° and 35°, were considered at both α= 10° and α= 30°. The nondimensional timestep used for all cases was 0.00262. A comparison of rolling moment coefficient versus roll angle for each of these cases is shown in Fig. 5 to illustrate the effects of both roll amplitude and angle of attack. For the α= 10° angle of attack cases shown in Fig. 5(a), the results show a counter-clockwise-oriented loop for each roll amplitude which would produce a convergent (stable) response if the wing were free to roll. This prediction of a stable response at the smallest roll amplitude is consistent with the pulse transfer-function results of Fig. 4(a). Also as the roll amplitude is increased from ϕ_0 = 5° to 15°, the rolling moment coefficient increases linearly. (Note the change in scaling of the vertical axis.) However, as the roll amplitude is further increased to ϕ_0 = 35°, some nonlinear aerodynamic

characteristics are exhibited in the "pinching" of the loop at the extreme roll angles although the free-to-roll response is still predicted to be stable. For the α= 30° angle of attack cases shown in Fig. 5(b), the results show clockwise-oriented loops for the ϕ_o = 5° and 15° roll amplitudes which would produce a divergent (unstable) response if the wing were free to roll. This prediction of an unstable free-to-roll response at the smaller roll amplitudes is consistent with the pulse transfer-function results of Fig. 4(b). At ϕ_o = 35°, counter-clockwise-oriented loops have formed at the extreme roll angles which consequently, would have a stabilizing effect on the free-to-roll response. The formation of these stabilizing loops was not, of course, predicted by the pulse analysis. In contrast with the α= 10° angle of attack case, at the higher angle of attack of 30°, the nonlinear aerodynamic effects at the larger roll amplitudes result in a change in the stability characteristics of the wing.

Free-to-Roll Results

The free-to-roll results were obtained for the flow conditions and structural and inertial parameter values listed in Table 1. The structural and inertial properties used in these calculations are loosely based on the characterisitcs of the models used in the experimental study of wing rock in Ref. 9. The initial angular velocity imposed on the wing was ϕ'= 0.003 and the nondimensional timestep used was 0.004. The resulting roll angle response, shown in Fig. 6(a) for the α= 10° case, indicates that after the initial perturbation, the oscillatory response converges to its initial steady-state value. This stable free-to-roll response is consistent with the pulse and forced harmonic results of Figs. 4(a) and 5(a). The roll angle response, shown Fig. 6(b), for the α= 30° case, indicates that initially the oscillatory response diverges for small values of roll amplitude which is consistent with the small amplitude pulse and harmonic results of Figs. 4(b) and 5(b). As the roll angle increases to around 35°, the rate of divergence decreases due to the stabilizing aerodynamics (counter-clockwise loops in the rolling moment coefficient at the extreme roll angles) shown in Fig. 5(b). Finally, the

response reaches a maximum amplitude of motion at approximately 38° corresponding to a limit cycle. The reduced frequency of the limit cycle is k = 0.103. These results are similar in nature to those obtained by Arena and Nelson[11] in a low-speed experimental investigation of wing rock. The wing- rock time history from Ref. 11, shown in Fig. 7, was obtained for an 80° swept delta wing at 30° angle of attack. The reduced frequency of the wing rock in this case was approximately 0.125. Although the case considered in the present study is different from that of Ref. 11 (the data from Refs. 8-12 are all for low speed flows whereas the conical Euler code is limited to supersonic freestream applications), the similarity between the two sets of results in Figs. 6(b) and 7 is noteworthy and gives credibility to the present calculations.

Active Roll-Suppression Results

An active rate-feedback control law was then implemented in an attempt to suppress the wing-rock motion. To determine an appropriate value for the gain, a stability analysis was derived by again recalling the nondimensional rolling equation of motion given by

$$\phi'' = C_1 C_\ell \tag{16}$$

Assuming that the rolling moment coefficient can be written as the superposition of the rolling moment coefficient transfer functions for ϕ and δ,

$$C_\ell = C_{\ell_\phi}\phi + C_{\ell_\delta}\delta \tag{19}$$

Substituting the control law from Eq. (15) into Eq. (19) gives

$$C_\ell = C_{\ell_\phi}\phi + C_{\ell_\delta}K_v\phi' \tag{20}$$

Then for simple harmonic motion

$$C_\ell = \{[\mathrm{Re}(C_{\ell_\phi}) - kM_\infty K_v \,\mathrm{Im}(C_{\ell_\delta})] + i[\mathrm{Im}(C_{\ell_\phi}) + kM_\infty K_v \,\mathrm{Re}(C_{\ell_\delta})]\}\phi \quad (21)$$

On the right-hand side of Eq. (21), as before, the first term represents an aerodynamic stiffness, and the second term represents an aerodynamic damping. Therefore, stabilizing the motion of the wing requires that

$$\mathrm{Im}(C_{\ell_\phi}) + k\, M_\infty K_v \,\mathrm{Re}(C_{\ell_\delta}) < 0 \quad (22)$$

Solving for the gain yields

$$K_v > \frac{-1}{kM_\infty} \quad \frac{\mathrm{Im}(C_{\ell_\phi})}{\mathrm{Re}(C_{\ell_\delta})} \quad (23)$$

A pulse analysis was performed to determine the rolling moment coefficient transfer function for δ at $\alpha = 30°$ angle of attack (pulse amplitude of $\delta_0 = 1°$). The transfer function from this analysis, shown in Fig. 8, indicates that for values of reduced frequency less than 0.5, the real part of C_{ℓ_δ} is negative. Considering Eq. (23) and recalling from Fig. 4(b) that the values of $\mathrm{Im}(C_{\ell_\phi})$ for k<0.5 are positive, the value of K_V must, therefore, be positive to suppress wing rock. The value of K_V actually needs to be greater than that determined by evaluating the right-hand side of Eq. (23) in order to stabilize the wing since the above analysis assumes simple harmonic motion. For the flow conditions considered here, for example, the value for the gain that produces a neutrally stable (or simple harmonic) response is $K_V = 0.35$. The free-to-roll analysis with active rate-feedback control was performed over a range of control gains: $K_V = 0.25$, 0.40, and 0.50. The time-histories of the wing motion are shown in Fig. 9. The time-history for a control gain of $K_V = 0.5$ indicates a damped response as expected. Similarly, the response for control gain of $K_V = 0.4$ is also damped although at a smaller rate than the $K_V = 0.5$ case. The response of the wing for a control gain of $K_V = 0.25$ shown in Fig. 9 indicates that the response is no longer damped. However, a comparison

with the results of Fig. 6(b) shows that the active rate-feedback control has a stabilizing effect on the free response at these conditions.

Concluding Remarks

A conical Euler code was developed to study unsteady vortex-dominated flows about rolling highly-swept delta wings, undergoing either forced or free-to-roll motions including active roll suppression. The flow solver of the code involved a multistage Runge-Kutta time-stepping scheme which uses a finite-volume spatial discretization of the Euler equations on an unstructured grid of triangles. The code allows for the additional analysis of the free-to-roll case, by including the rigid-body equation of motion for its simultaneous time integration with the governing flow equations. Results were presented for a 75° swept sharp-leading-edge delta wing at a freestream Mach number of 1.2 and at α = 10° and 30° angle of attack. At the lower angle of attack of α = 10°, for example, a forced harmonic motion produced a rolling moment coefficient versus roll angle response that is counter-clockwise in orientation. This counter-clockwise response is indicative of stability in roll which was verified in a free-to-roll calculation. In contrast, at the higher angle of attack of α = 30°, the forced harmonic response was clockwise in orientation which indicates instability in roll. A free-to-roll calculation for this case produced an initially divergent response, but as the amplitude of motion grew with time the response transitioned to a limit cycle phenomenon known as wing rock. The wing rocking motion was subsequently suppressed, however, through the use of an active rate-feedback control law and antisymmetrically-deflected leading-edge flaps.

Acknowledgement

The authors would like to acknowledge Ken Morgan and Jaime Peraire of the Imperial College of Science, Technology and Medicine, London, England, for providing the

advancing front method grid generation program that was used to generate the grid in the present study.

References

[1]High Angle of Attack Aerodynamics, AGARD-LS-121, December 1982; Lecture Series presented March 10-11, 1982 at NASA Langley Research Center, USA, March 15-19, 1982 at von Karman Institute, Rhode-Saint-Genese, Belgium, and March 22-23, 1982 at DFVLR, Gottingen, Germany.

[2]Vortex Flow Aerodynamics, NASA CP-2416, July 1986; Proceedings of a conference sponsored by the NASA Langley Research Center, Hampton, Virginia, and the Air Force Wright Aeronautical Laboratories, Flight Dynamics Laboratory, Wright-Patterson Air Force Base, Ohio; held at NASA Langley Research Center, October 8-10, 1985.

[3]Hamilton, W. T.: Manoeuvre Limitations of Combat Aircraft, AGARD-AR-155A, August 1979.

[4]Hummel, D.: Documentation of Separated Flows for Computational Fluid Dynamics Validation, AGARD-CP-437, Vol. 2, December 1988, pp. p15-1 to p15-24.

[5]Kjelgaard, S. O.; and Sellers, W. L.: Detailed Flowfield Measurements Over a 75° Swept Delta Wing for Code Validation, AGARD-CP-437, Vol. 2, December 1988, pp. p10-1 to p10-14.

[6]Squire, L. C.: Leading-Edge Separation and Cross Flow Shocks on Delta Wings, AIAA Journal, Vol. 23, March 1985, pp. 321-325.

[7]Miller, D. S.; and Wood, R. M.: Lee-Side Flow Over Delta Wings at Supersonic Speeds, NASA TP-2430, June 1985.

[8]Nguyen, L. T.; Yip, L.; and Chambers, J. R.: Self-Induced Wing Rock of Slender Delta Wings, AIAA Paper No. 81-1883, August 1981.

[9]Levin, D.; and Katz, J.: Dynamic Load Measurements with Delta Wings Undergoing Self-Induced Roll Oscillations, Journal of Aircraft, Vol. 21, January 1984, pp. 30-36.

[10]Jun, Y. W.; and Nelson, R. C.: Leading-Edge Vortex Dynamics on a Slender Oscillating Wing, Journal of Aircraft, Vol. 25, September 1988, pp. 815-819.

[11]Arena, A. S.; and Nelson, R. C.: The Effect of Asymmetric Vortex Wake Characteristics on a Slender Delta Wing Undergoing Wing Rock Motion, AIAA Paper No. 89-3348, August 1989.

[12]Ng, T. T.; Malcolm, G. N.; and Lewis, L. C.: Flow Visualization Study of Delta Wings in Wing-Rock Motion, AIAA Paper No. 89-2187, August 1989.

[13]Hoeijmakers, H. W. M.: Computational Vortex Flow Aerodynamics, AGARD-CP-342, Aerodynamics of Vortical Type Flows in Three Dimensions, July 1983, pp. 18-1 to 18-35.

[14]Newsome, R. W.; and Kandil, O. A.: Vortical Flow Aerodynamics - Physical Aspects and Numerical Simulation, AIAA Paper No. 87-0205, January 1987.

[15]Hsu C. H.; and Lan, C. E.: Theory of Wing Rock, Journal of Aircraft, Vol. 22, October 1985, pp. 920-924.

[16]Konstadinopoulos, P.; Mook, D. T.; and Nayfeh, A. H.: Subsonic Wing Rock of Slender Delta Wings, Journal of Aircraft, Vol. 22, March 1985, pp. 223-228.

[17]Elzebda, J. M.; Nayfeh, A. H.; and Mook, D. T.: Development of an Analytical Model of Wing Rock for Slender Delta Wings, Journal of Aircraft, Vol. 26, August 1989, pp. 737-743.

[18]Nayfeh, A. H.; Elzebda, J. M.; and Mook, D. T.: Analystical Study of the Subsonic Wing-Rock Phenomenon for Slender Delta Wings, Journal of Aircraft, Vol. 26, September 1989, pp. 805-809.

[19]Newsome, R. W.; and Thomas, J. L.: Computation of Leading-Edge Vortex Flows, Proceedings of the Conference on Vortical Flow Aerodynamics, NASA Langley Research Center, Hampton, Virginia, October 8-10, 1985.

[20]Kandil, O. A.; and Chuang, A.: Influence of Numerical Dissipation in Computing Supersonic Vortex-Dominated Flows, AIAA Paper No. 86-1073, May 1986.

[21]Chakravarthy, S. R.; and Ota, D. K.: Numerical Issues in Computing Inviscid Supersonic Flow Over Conical Delta Wings, AIAA Paper No. 86-0440, January 1986.

[22]Murman, E. M.; Powell, K. G.; Miller, D. S.; and Wood, R. M.: Comparisons of Computations and Experimental Data for Leading Edge Vortices - Effects of Yaw and Vortex Flaps, AIAA Paper No. 86-0439, January 1986.

[23]Murman, E. M.; and Rizzi, A.: Applications of Euler Equations to Sharp Edge Delta Wings With Leading Edge Vortices, AGARD-CP-412, November 1986.

[24]McMillin, S. N.; Thomas, J. L.; and Murman, E. M.: Euler and Navier-Stokes Solutions for the Leeside Flow Over Delta Wings at Supersonic Speeds, AIAA Paper No. 87-2270, July 1987.

[25]Fujii, K.: A Method to Increase the Accuracy of Vortical Flow Simulations, AIAA Paper No. 88-2562, July 1988.

[26]Powell, K. G.; Murman, E. M.; Perez, E. S.; and Baron, J. R.: Total Pressure Loss in Vortical Solutions of the Conical Euler Equations, AIAA Journal, Vol. 25, 1987.

[27]Kandil, O. A.; and Chuang, A. H.: Computation of Steady and Unsteady Vortex Dominated Flows, AIAA Paper No. 87-1462, June 1987.

[28]Kandil, O. A.; and Chuang, A. H.: Unsteady Navier-Stokes Computations Past Oscillating Delta Wing at High Incidence, AIAA Paper No. 89-0081, January 1989.

[29]Batina, J. T.: Vortex-Dominated Conical-Flow Computations Using Unstructured Adaptively-Refined Meshes, AIAA Paper No. 89-1816, June 1989.

[30]Lee, E. M.; and Batina, J. T.: Conical Euler Solution for a Highly-Swept Delta Wing Undergoing Wing-Rock Motion, NASA TM 102609, March 1990.

[31]Karagonnis, T.; Maxworthy, T.; and Spedding, G. R.: Generation and Control of Separated Vortices Over a Delta Wing by Means of Leading Edge Flaps, AIAA Paper No. 89-0997, March 1989.

[32]Ng, T. T.: On Leading Edge Vortex and Its Control, AIAA Paper No. 89-3346, August 1989.

[33]Wood, N. J.; Roberts, L.; and Celik, Z.: The Control of Asymmetric Vortical Flows Over Delta Wings at High Angles of Attack, AIAA Paper No. 89-3347, August 1989.

[34]Ellis, D. G.; and Stollery, J. L.: The Behavior and Performance of Leading-Edge Vortex Flaps, ICAS-88-4.5.2, 1988.

[35]Batina, J. T.: Unsteady Euler Airfoil Solutions Using Unstructured Dynamic Meshes, AIAA Paper No. 89-0115, January 1989.

[36]Seidel, D. A.; Bennett, R. M.; and Whitlow, W., Jr.: An Exploratory Study of Finite Difference Grids for Transonic Unsteady Aerodynamics, AIAA Paper No. 83-0503, January 1983.

[37]Seidel, D. A.; Bennett, R. M.; and Ricketts, R. H.: Some Recent Applications of XTRAN3S, AIAA Paper No. 83-1811, July 1983.

[38]Morgan, K.; and Peraire, J.: Finite Element Methods for Compressible Flow, Von Karmen Institute for Fluid Dynamics Lecture Series 1987-04, Computational Fluid Dynamics, March 2-6, 1987.

Table 1 Summary of structural parameter values and flow conditions for the free-to-roll calculation.

Parameter	Value
c	0.2820 m
I_{xx}	0.1776 x 10^{-3} Kg m^2
μ_x	0.0 Kg m^2/s
ρ_∞	0.526 Kg/m^3
a_∞	312 m/s

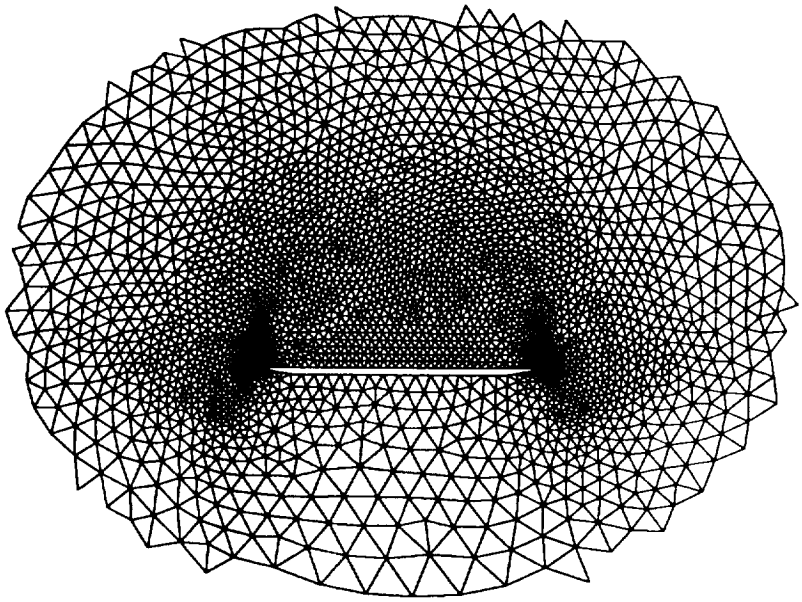

Fig. 1 Partial view of unstructured grid about a 75° swept delta wing.

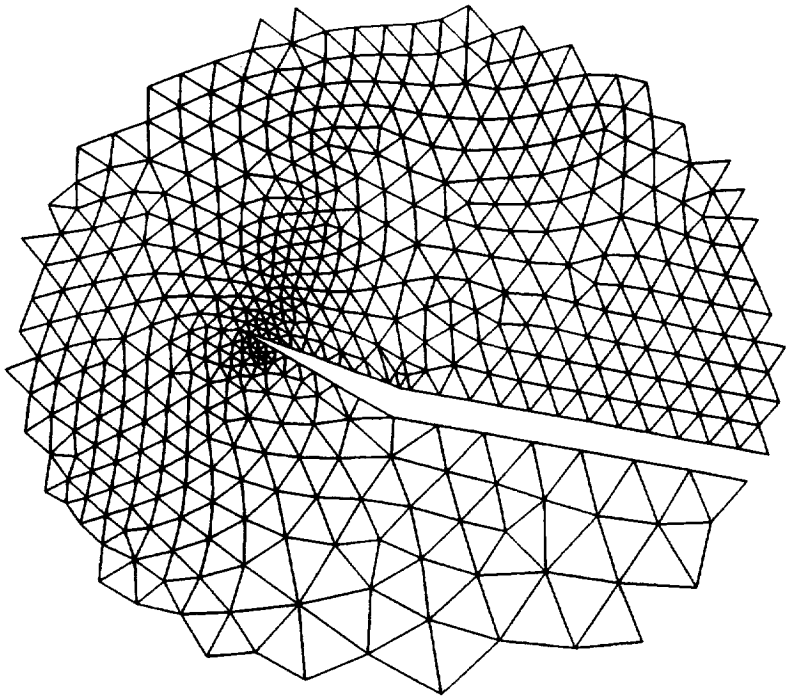

(a) $\delta = 10°$.

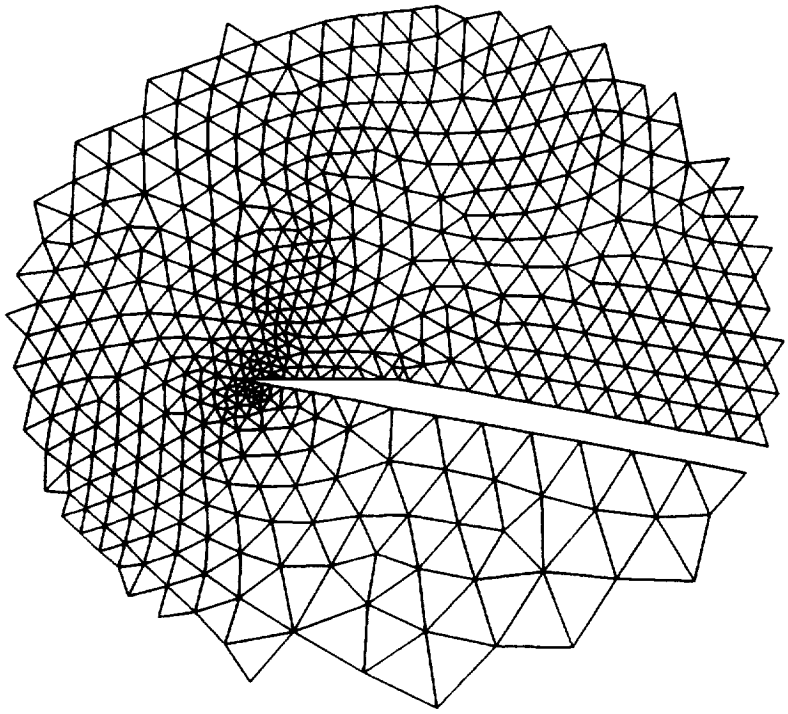

(b) $\delta = -10°$.

Fig. 2 Partial view of deforming mesh about deflected leading-edge flap.

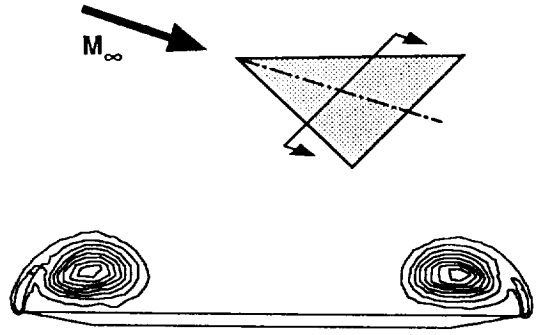

(a) $\alpha = 10°$.

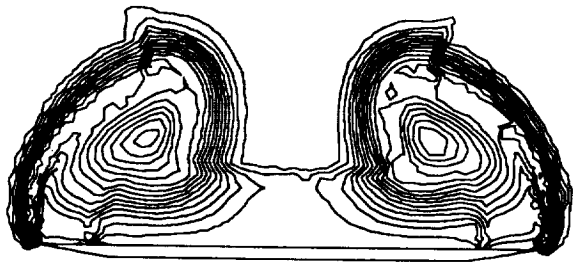

(b) $\alpha = 30°$.

Fig. 3 Angle of attack effects on steady state total pressure loss contours for a 75° swept delta wing at $M_\infty = 1.2$.

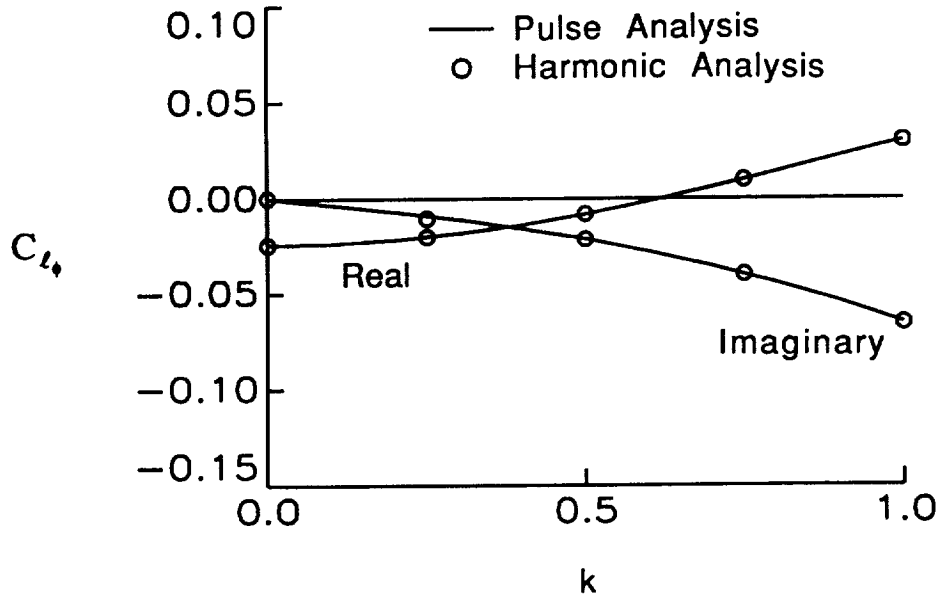

(a) $\alpha = 10°$.

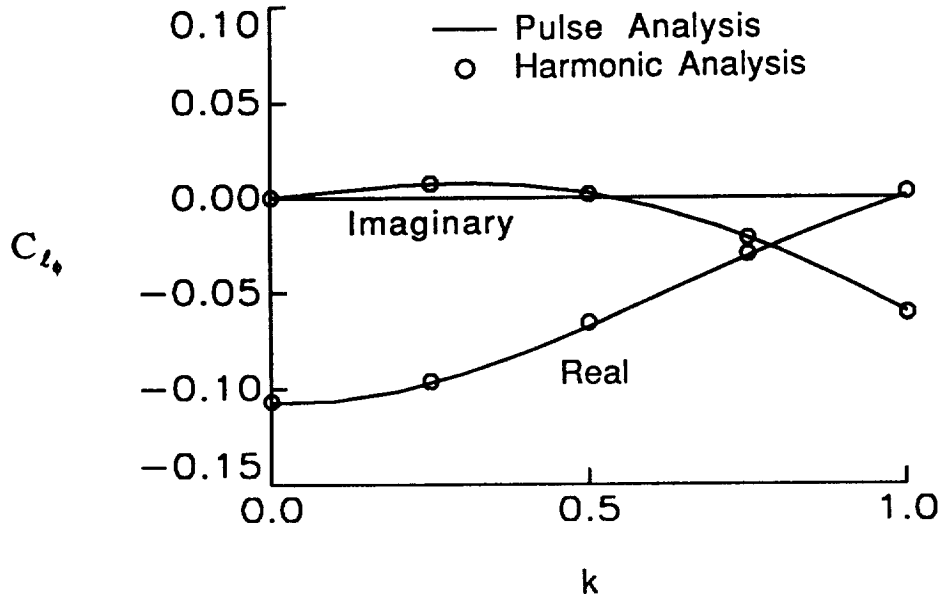

(b) $\alpha = 30°$.

Fig. 4 Angle of attack effects on the rolling moment coefficient transfer-function versus reduced frequency for a 75° swept delta wing at $M_\infty = 1.2$ (pulse amplitude $\phi_0 = 1°$).

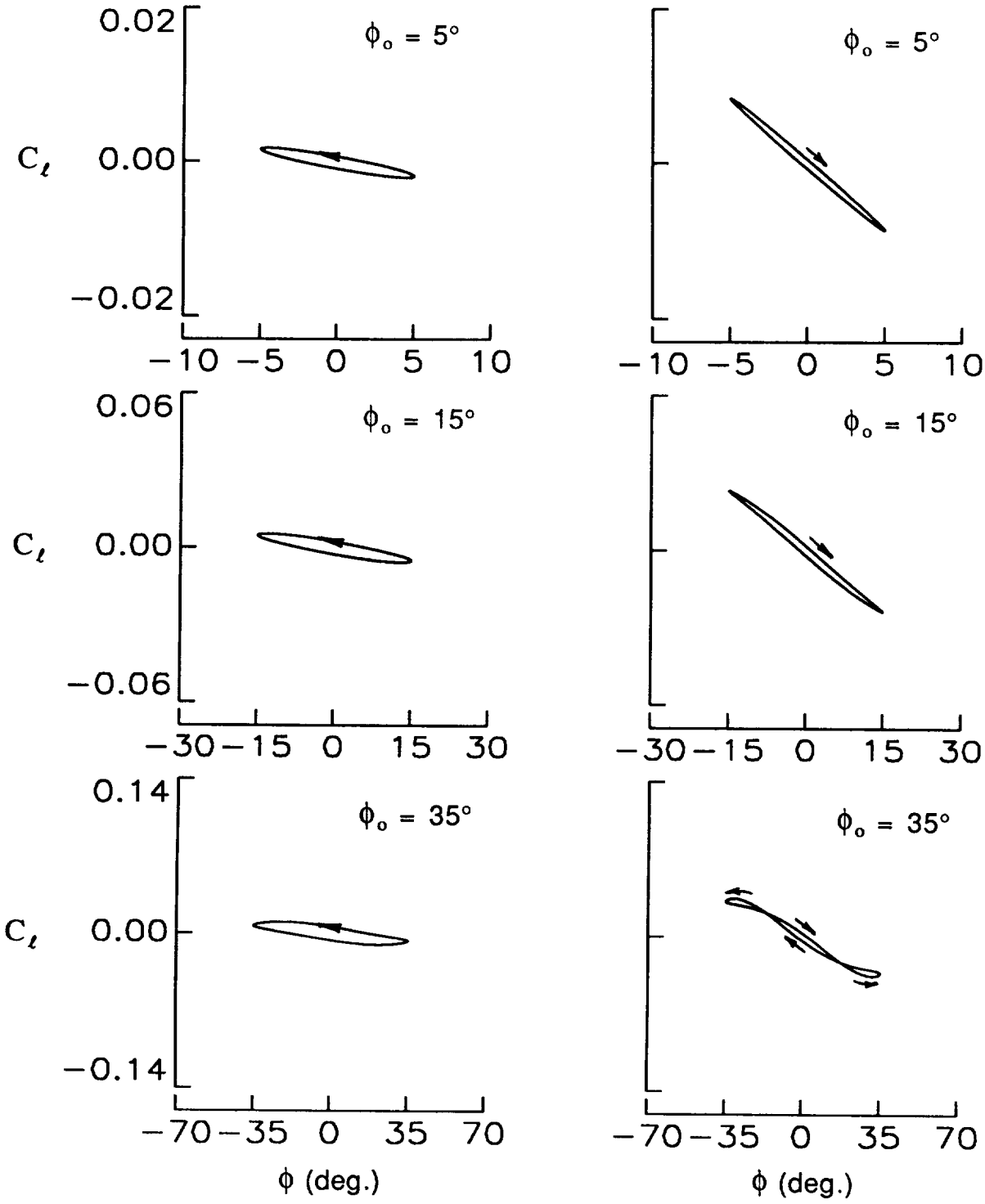

Fig. 5 Angle of attack effects on the rolling moment coefficient versus instantaneous roll angle for a 75° swept delta wing at M_∞ = 1.2 and k = 0.25.

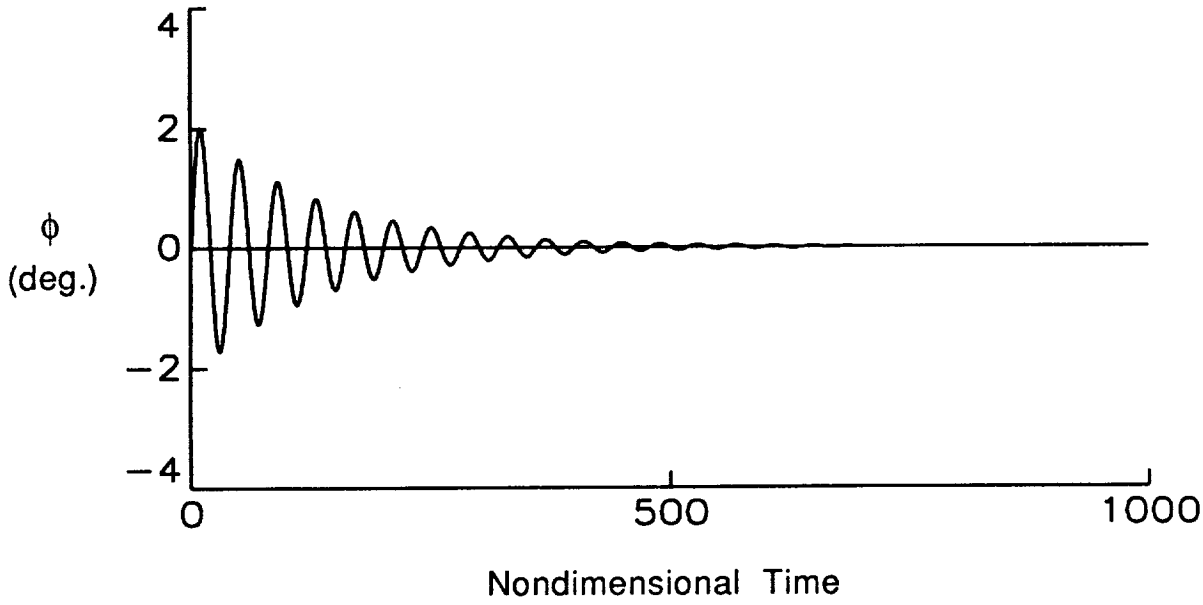

(a) α = 10°.

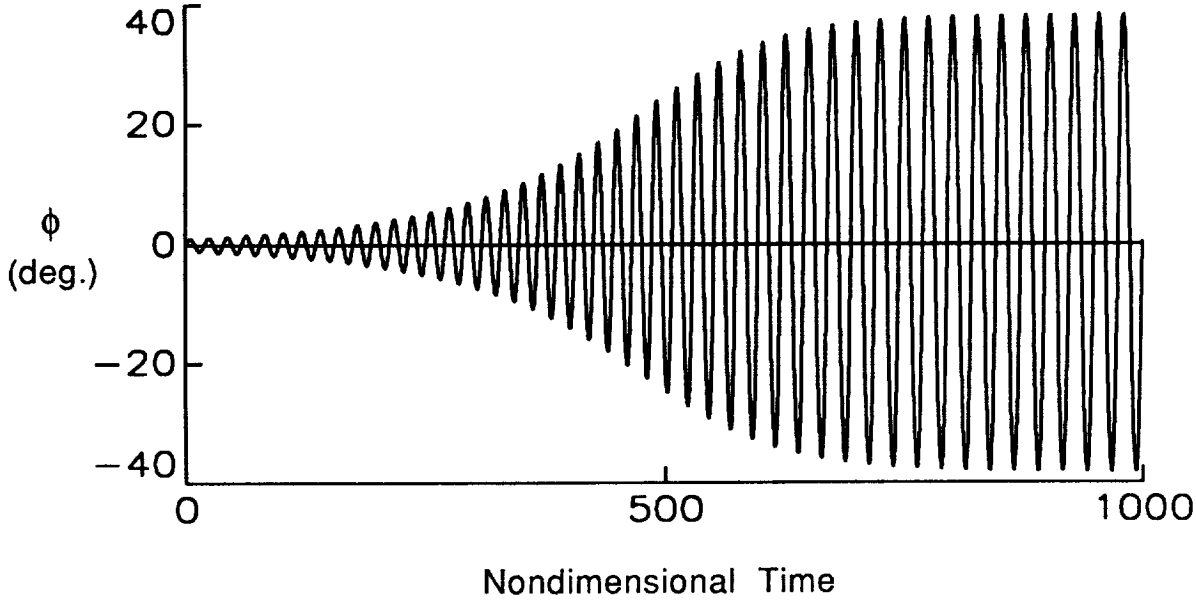

(b) α = 30°.

Fig. 6 Angle of attack effects on free-to-roll response for a 75° swept delta wing at M_∞ = 1.2.

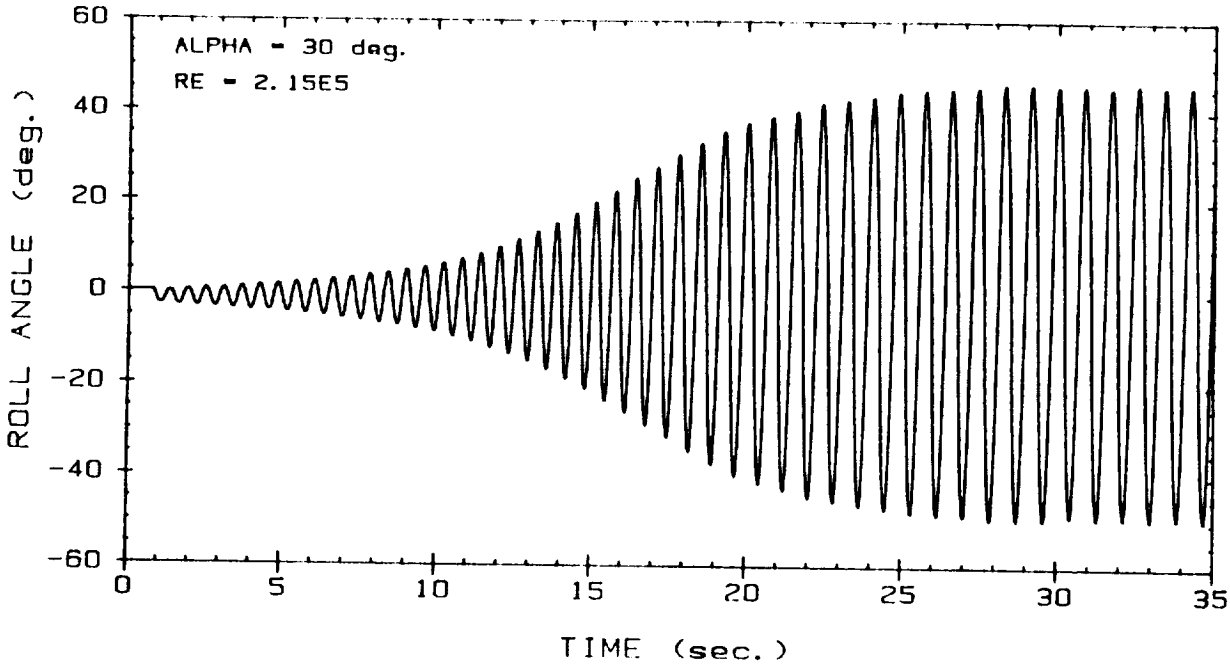

Fig. 7 Wing-rock time history for an 80° swept delta wing at 30° angle of attack (Ref. 11, reprinted with permission from Professor Robert C. Nelson, Notre Dame University).

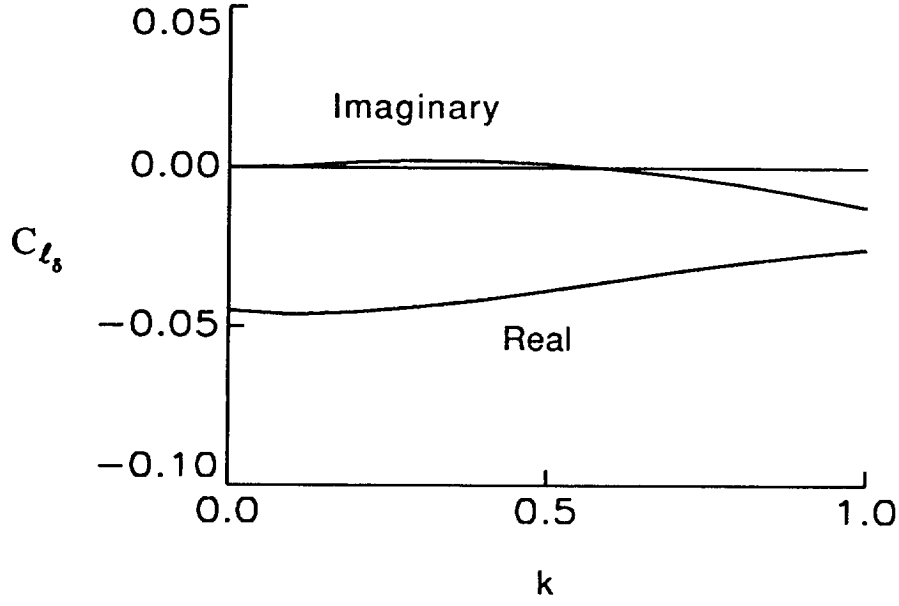

Fig. 8 Rolling moment coefficient transfer-function for the flap versus reduced frequency for a 75° swept delta wing at $M_\infty = 1.2$ (pulse amplitude $\delta_0 = 1°$).

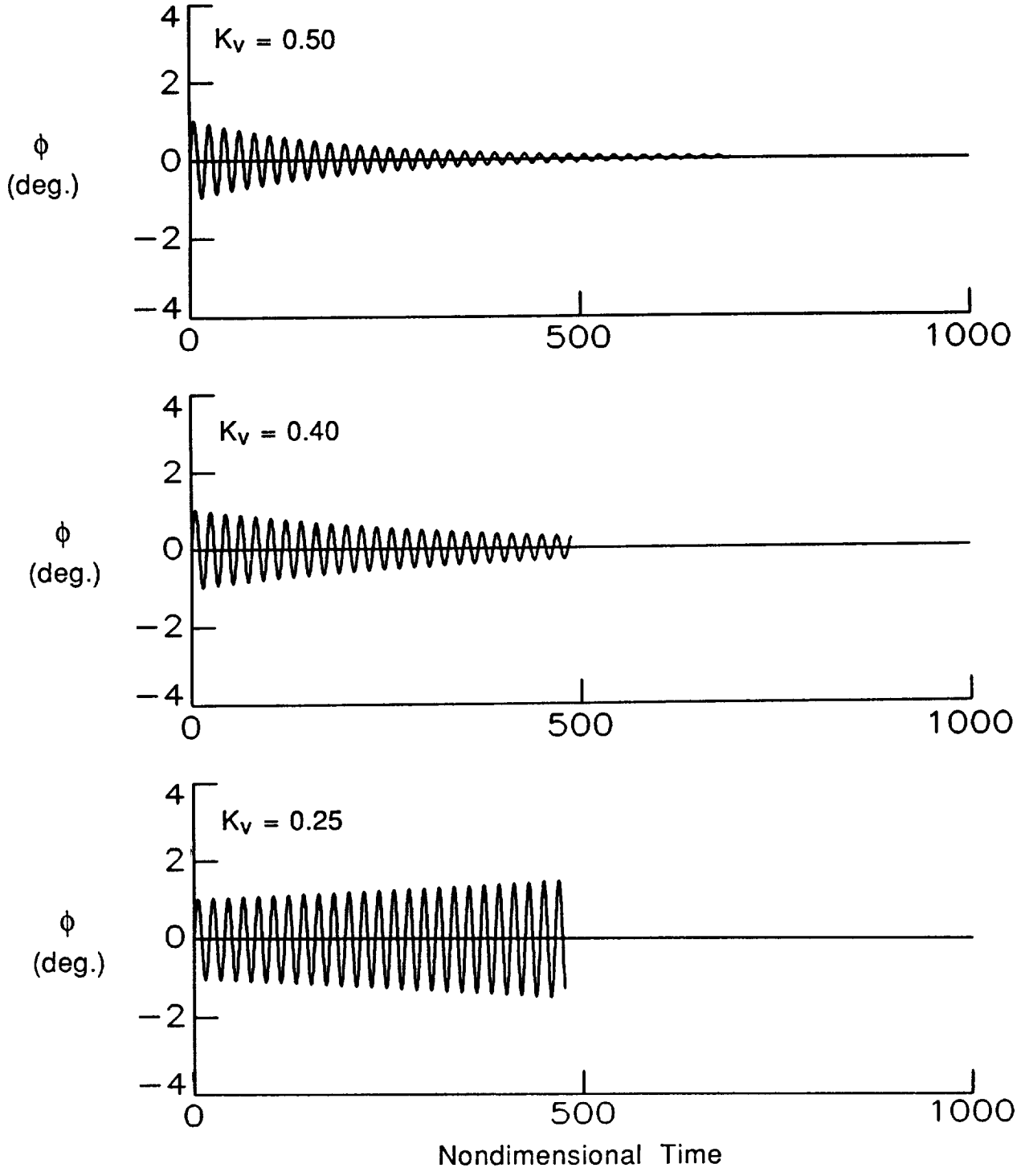

Fig. 9 Free-to-roll response with rate-feedback control for a 75° swept delta wing at M_∞ = 1.2 and α = 30°.

NASA
National Aeronautics and Space Administration

Report Documentation Page

1. Report No.	2. Government Accession No.	3. Recipient's Catalog No.
NASA TM-102683		

4. Title and Subtitle	5. Report Date
Conical Euler Simulation and Active Suppression of Delta Wing Rocking Motion	October 1990
	6. Performing Organization Code

7. Author(s)	8. Performing Organization Report No.
Elizabeth M. Lee and John T. Batina	
	10. Work Unit No. 505-63-21-01

9. Performing Organization Name and Address	11. Contract or Grant No.
NASA Langley Research Center Hampton, Virginia 23665-5225	
	13. Type of Report and Period Covered

12. Sponsoring Agency Name and Address	13. Type of Report and Period Covered
National Aeronautics and Space Administrations Washington, DC 20546	Technical Memorandum
	14. Sponsoring Agency Code

15. Supplementary Notes

16. Abstract

A conical Euler code was developed to study unsteady vortex-dominated flows about rolling highly-swept delta wings, undergoing either forced or free-to-roll motions including active roll suppression. The flow solver of the code involves a multistage Runge-Kutta time-stepping scheme which uses a finite-volume spatial discretization of the Euler equations on an unstructured grid of triangles. The code allows for the additional analysis of the free-to-roll case, by including the rigid-body equation of motion for its simulataneous time integration with the governing flow equations. Results are presented for a 75° swept sharp-leading-edge delta wing at a freestream Mach number of 1.2 and at $\alpha = 10°$ and 30° angle of attack. At the lower angle of attack of $\alpha = 10°$, a forced harmonic analysis indicates that the rolling moment coefficient provides a positive damping which is verified in a free-to-roll calculation. In contrast, at the higher angle of attack of $\alpha = 30°$, a forced harmonic analysis indicates that the rolling moment coefficient provides a negative damping at the small roll amplitudes. A free-to-roll calculation for this case produces an initially divergent response, but as the amplitude of motion grows with time, the response transitions to a wing-rock type of limit cycle oscillation. The wing rocking motion may be actively suppressed, however, through the use of a rate-feedback control law and antisymmetrically-deflected leading-edge flaps. The paper provides descriptions of the conical Euler flow solver and the free-to-roll analysis. Results are presented which give insight into the flow physics associated with unsteady vortical flows

17. Key Words (Suggested by Author(s))	18. Distribution Statement
Wing Rock Computational Fluid Dynamics Unsteady Aerodynamics Vortical Flow Active Control	Unclassified - Unlimited Subject Category - 02

19. Security Classif. (of this report)	20. Security Classif. (of this page)	21. No. of pages	22. Price
Unclassified	Unclassified	33	A03